J Nanostruct 15(4): 2590-2613, Autumn 2025

RESEARCH PAPER

Effect of Deposition Conditions on Structural, Optical, and Electrical Properties of NiO Thin Films Prepared by Spray Pyrolysis

Abas Javadian, Mohammad Reza Fadavieslam *

School of Physics, Damghan University, Damghan, Iran

ARTICLE INFO

Article History:
Received 05 June 2025
Accepted 27 September 2025
Published 01 October 2025

Keywords:
Deposition conditions
Nickel oxide
Spray pyrolysis
Thin film

ABSTRACT

Thin films of Nickel oxide were successfully deposited at different substrate temperatures (440, 460, 480, and 500 °C), solution volumes (50, 100, 150, and 200 ml), and spray rates (1, 2.5, 5, and 7.5 ml/min) on soda-lime glass substrates using $NiCl_2.6H_2O$ as a precursor at a concentration of 0.1 M and the spray pyrolysis technique. The structural, optical, and electrical properties of the thin films were characterized. They show a polycrystalline nature with a cubic structure of single-phase NiO and peaks related to (111), (200), and (220) with a preferential orientation along (111). The morphology of NiO thin films resembles that of spherical grains on the entire surface and an average roughness ranging from 28.71 to 84.54 nm. It depends on the deposition conditions. The absorption coefficient, refractive index, extinction coefficient, dielectric constants and optical conductivity were all calculated in the range of (300 and 1100 nm). The range of optical gap, Urbach energy, electrical resistivity, carrier concentration, and carrier mobility were measured to be 2.66 to 3.49 eV, 0.41 to 0.6 eV, 1.33×10^3 to 2.96×10^3 Ω.cm, 1.42×10^{14} to 3.64×10^{14} cm^{-3}, and 8.21 to 24.25 cm^2/v.s, respectively, as a function of deposition conditions. As the Hall effect studies showed, the films exhibited p-type conductivity.

How to cite this article
Javadian A., Fadavieslam M. Effect of Deposition Conditions on Structural, Optical, and Electrical Properties of NiO Thin Films Prepared by Spray Pyrolysis. J Nanostruct, 2025; 15(4):2590-2613. DOI: 10.22052/JNS.2025.04.093

INTRODUCTION

Since transparent conducting oxides (TCOs) have high transmittance and low resistivity, they are widely used in research, especially in the optoelectronics industry [1-3]. Most of them have n-type conductivity [4, 5]. However, nickel oxide is a transparent conductive oxide material with p-type conductivity [6]. The reason is that although pure stoichiometric NiO is an insulator with a resistivity at room temperature in the order of 10^{13} Ω cm, nonstoichiometric NiO exhibits p-type conductivity because of the presence of Ni^{3+} ions resulting from Ni^{2+} vacancies and/or interstitial oxygen in NiO crystallites [7-9]. In other words, Ni vacancies form easily and act as acceptors [10]. Among other properties, it has a wide band gap of 3.6 to 4 eV, NaCl crystal structure, high chemical ductility and stability, excellent durability, and low material cost [11-15]. These properties give NiO good optical, electrical, thermoelectric, and catalytic properties [4, 16]. The assets of NiO depend solely on the ratio of nickel to oxygen atoms [12]. The properties of nickel oxide make it a promising candidate for numerous applications such as supercapacitors [17], antireflection coatings [4], solar thermal absorber [18], the catalyst for the evaluation of

* *Corresponding Author Email: m.r.fadavieslam@du.ac.ir*

This work is licensed under the Creative Commons Attribution 4.0 International License.
To view a copy of this license, visit http://creativecommons.org/licenses/by/4.0/.

oxygen [19], gas sensors [20], fuel cell electrodes [21], energy-efficient smart windows [22], random access memory devices [23], organic light-emitting diodes [8], electrochromic device [24], surface acoustic devices [25], UV photodetectors [26], thermoelectric devices [27], and so on.

NiO thin films have been deposited by various methods, e.g. by thermal evaporation [28], electron beam evaporation [29], physical-vapor [30], pulsed laser deposition [31], sputtering [32], atomic layer [33], electrochemical [34], spin coating [35], dip-coating method [36], successive ionic layer adsorption and reaction (SILAR) [37], chemical vapor deposition [38], bath deposition (CBD) [39], and spray pyrolysis [40]. Chemical spray pyrolysis is a non-complicated, fast, and low-cost process for producing thin films with the capacity to uniformly cover larger areas [7, 13]. The substrate temperature, spray rate, and solution volume are preparation conditions that can greatly affect the film properties. The behavior of NiO thin films strongly depends on their stoichiometric ratio of nickel to oxygen atoms, which can be controlled by the thin film preparation conditions [8]. The effect of substrate temperature [13, 19], solution volume [41, 42], and spray rate [43] on the physical properties of nickel oxide thin films prepared by thermal spraying have been studied separately by researchers. Nevertheless, the examination of the conducted research shows that a systematic review of all the mentioned factors on the properties of nickel oxide thin films has not been reported. Therefore, NiO thin films were prepared here by spray pyrolysis, and the structural, optical, and electrical properties of the films were investigated as a function of substrate temperature, solution volume and spray rate.

MATERIALS AND METHODS

Film preparation

For each thin film deposition, the molarity of nickel in the spray solution was 0.1 M. For example, 100 ml of spray solution was prepared by dissolving 2.3769 g of nickel chloride [$NiCl_2.6H_2O$] in 100 ml of deionized water. Each solution was stirred well and heated at room temperature for approximately 45 minutes until it was bright and ready for spraying. The solutions were applied to a soda lime substrate under similar conditions: 30 cm distance between the nozzle and the substrate, 30 rpm rotation speed of the hot plate, and 3 atm pressure of the carrier gas, but at different substrate temperatures, solution volumes, and spray rates as shown in Table 1. To investigate the effect of substrate temperature, the temperature of the substrate was changed in a range of 440-500 °C with a step of 20 °C and an accuracy of ± 2 °C and a digital temperature controller was used to control it. Second, the effect of the solution volume on the physical properties of the thin films was investigated. The solution volumes were chosen to be 50, 100, 150, and 200 ml. To investigate the effects of the spray rate on the thin films, 1, 2.5, 5, and 7.5 mL/min were chosen. The glass substrates had been cleaned with ethanol in an ultrasonic bath for 15 minutes and placed on a hot plate, before the films were prepared. At the end, the system was allowed to cool to room temperature for approximately 80 minutes. In order to prepare the thin film a typical spray pyrolysis coating system was used [44].

Sample characterization

The crystal structures of the thin films were characterized using the XRD technique. The XRD instrument was a D8 Advance Bruker X-ray diffractometer with a Cu tube producing Cu-Ka radiation (k = 0.154056 nm) in a 2θ range of 10o-90o. The surface morphology of the samples was observed via FE-SEM using MIRA3 TESCAN. The cross-sectional FE-SEM image was also used to estimate the thickness of the thin films. The topology of the films was observed using an ARA AFM Ara Research Co. (Model No: 0201A) atomic force microscope (AFM). The transmittance and reflectance spectra of the thin films were measured using the UV-Vis. (300-1100 nm) spectrophotometer, Shimadzo-1800. An Ecopia

Table 1. Spray deposition parameters for the preparation of NiO thin films.

	Effect of substrate temperature	Effect of spray rate	Effect of solution volume
Substrate temperature (°C)	440, 460, 480, 500	460	460
Spray rate (mL/min)	2.5	1, 2.5, 5, 7.5	2.5
Solution volume (mL)	100	100	50, 100, 150, 200

CC BY

HMS-7000 Photonic Hall Effect Measurement System was used for the electrical measurement.

RESULTS AND DISCUSSION

Structural characterization

Figs. 1, 2, and 3 show the XRD patterns of the films deposited at different substrate temperatures, solution volumes, and spray rates, respectively. As you can see, plentiful diffraction peaks in the diffraction patterns show a polycrystalline nature with a cubic phase and preferential orientation along the (1 1 1) direction of the pure NiO phase, and no other phase could be noticed [45-49]. Some weak reflection peaks were also detected, such as (2 0 0) and (2 2 0), which could be related to poor crystallization [46]. Peaks (1 1 1), (2 0 0) and (2 2 0) are located at 37.29°, 43.67°, and 6373° for all thin films, respectively. The obtained diffraction peaks agree well with the JCPDS Card Number 14-0481 [12]. All samples show the same structural pattern with only the intensity differences. This could be a good indicator of the crystallinity of the film [12]. This indicates that the NiO phase is stable, and its formation is independent of the deposition parameters of the thin films [50].

The XRD thin films deposited at substrate temperatures of 440, 460, 480, and 500 °C are shown in Fig. 1. The figure shows that as the substrate temperature increases, the intensity of the peaks decreases [12]. This can be due to, at a low substrate temperature, a suitable chemical reaction takes place to form a NiO thin film on the substrate. Moreover, at a substrate temperature of 440 °C, enlargement and densification of the grains occur [12]. In contrast, increasing the substrate temperature above 440 °C would result in the spray solution receiving more thermal energy than required to form the crystalline structure of the nickel oxide phase, which could be because of homogeneous reaction and incomplete thermal decomposition, reducing the crystallinity of the thin films [12]. The apparent decrease in the intensity of the diffraction peaks at higher temperatures is also related to the deterioration of the crystallinity, and the strain produced [51]. As a result, a small number of nucleation centers begin to grow, resulting in larger grains as the temperature increases. The thickness of the film decreases, which is typical of the spraying process where the spray droplets are driven away from the reaction zone, and only a few precursors reach the substrate [12, 52].

Fig. 2 shows the XRD of thin films prepared with 50, 100, 150, and 200 ml solution volumes. The size of the main XRD peak corresponding to the (1 1 1) plane and the value of the area under the peak improve slightly as film thickness increases [50, 53, 54]. From the general observations, it is clear that the solution volume plays a crucial role in the crystallinity of the nickel oxide film [50, 53,

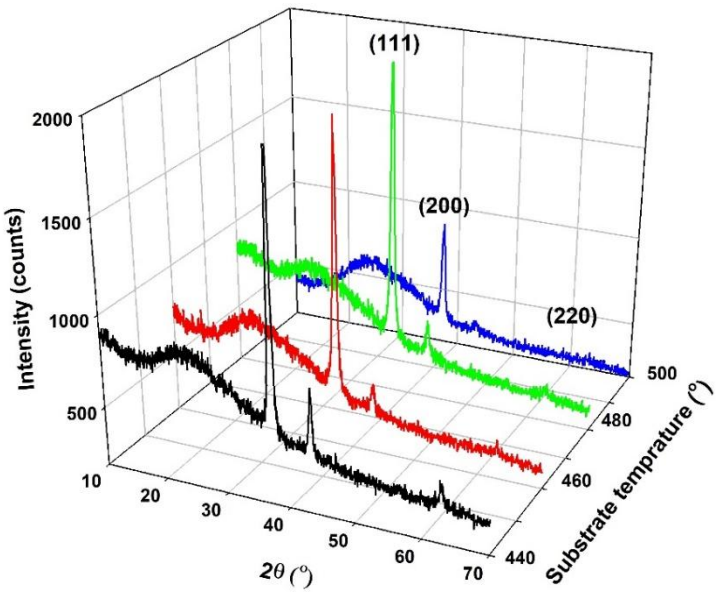

Fig. 1. The XRD patterns for the NiO thin films at different substrate temperatures.

CC BY

54]. A closer look at Fig. 3 shows that as the spray rate increases, the intensity of the peaks indicates lower crystallinity. At a low spray rate, there is less grain fluctuation, and the thin film has the opportunity to improve its crystal structure.

The NiO crystallizes in the cubic structure. The

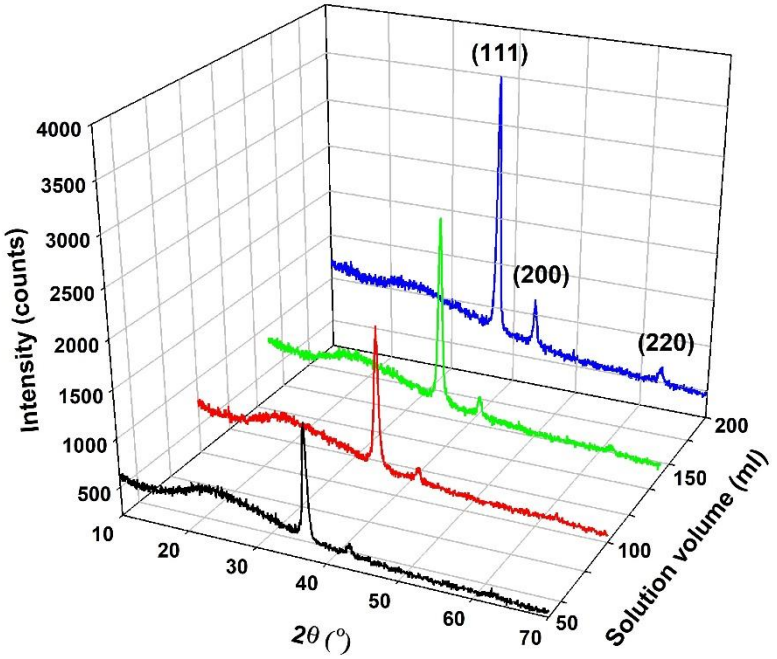

Fig. 2. The XRD patterns for the NiO thin films at different solution volumes.

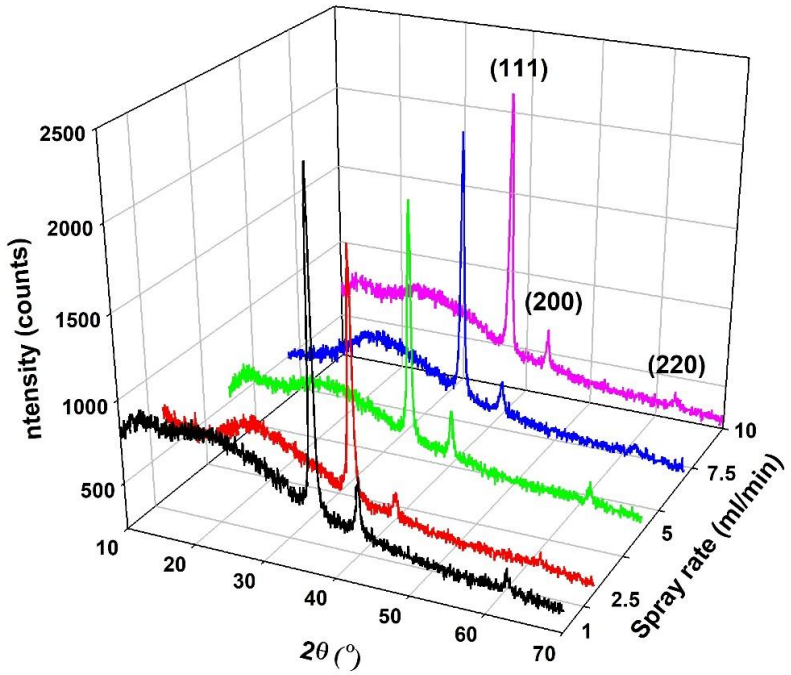

Fig. 3. The XRD patterns for the NiO thin films at different spray rates.

CC BY

interplanar spacings of the given Miller indices h, k, and l, d_{hkl} values of the NiO thin films were also calculated using the Bragg equation:

$$2d_{hkl}\sin\theta = n \quad (1)$$

where n is the diffraction order (usually n = 1) and λ is the x-ray wavelength. The lattice constant (a) was calculated using the following equation [47]:

$$\frac{1}{d_{hkl}^2} = \frac{h^2 + k^2 + l^2}{a^2} \quad (2)$$

Lattice parameter a for the cubic phase was calculated by (1 1 1) orientations. The average crystal grain size (D) was estimated by [55]:

$$D = \frac{0.94\lambda}{\beta\cos\theta} \quad (3)$$

and the dislocation density (δ) and strain (ε) were calculated using the following relations [13]:

$$\delta = \frac{1}{D^2} \quad (4)$$

$$\varepsilon = \frac{\beta\cos\theta}{4} \quad (5)$$

where ϑ is the usual Bragg angle, and β is the full width at half maxima of the diffraction peaks. The structural parameters for (111) the crystallographic orientation of the deposited NiO thin films is summarized in Table 2. The observed 'd' and 'a' values agree well with the standard 'd' and 'a' values Fig. 4 shows the differences in average crystal grain size as a function of substrate temperatures, solution volumes, and spray rates. It can be seen from Fig. 4 that the average crystal

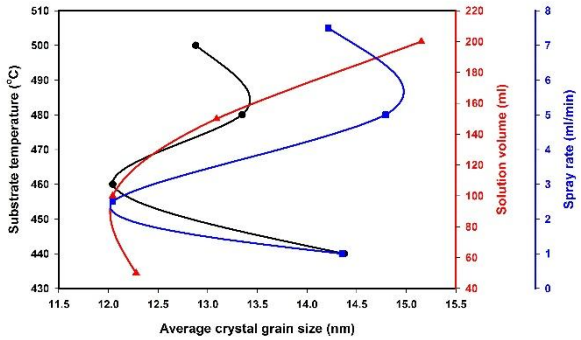

Fig. 4. Variations in average crystal grain size as a function of substrate temperature, solution volume and spray rate.

Table 2. The results of structural characterization of the thin films.

Sample	2θ (°)	FWHM (°)	Observed 'd' values (nm)	Observed 'a' values (nm)	D (nm)	δ×10^{15} (lines/m^2)	ε×10^{-3} (lines^2 m^4)	average roughness (nm)
Substrate temperature (o)								
440	37.295	0.609	2.40912	4.17259	14.378	4.84	2.52	62.65
460	37.261	0.727	2.41124	4.17626	12.043	6.89	3.01	57.71
480	37.257	0.656	2.41145	4.17663	13.347	5.61	2.71	46.2
500	37.332	0.68	2.40678	4.16854	12.879	6.03	2.81	36.15
Solution volume (ml)								
50	37.226	0.713	2.4138	4.18070	12.279	6.63	2.95	28.71
100	37.261	0.727	2.41124	4.17626	12.043	6.89	3.01	57.71
150	37.273	0.669	2.41048	4.17495	13.089	5.84	2.77	78.64
200	37.323	0.578	2.40736	4.16954	15.151	4.36	2.39	84.54
Spray rate (ml/min)								
1	37.262	0.61	2.41119	4.17618	14.354	4.85	2.52	71.24
2.5	37.261	0.727	2.41124	4.17626	12.043	6.89	3.01	57.71
5	37.278	0.592	2.41018	4.174431	14.791	4.57	2.45	39.27
7.5	37.285	0.616	2.4097	4.173600	14.215	4.95	2.55	68.48

CC BY

grain size decreases as the substrate temperature increases. It also shows that as the solution volume increases, so does the average crystal grain size increase. These results indicate that increasing the solution volume improves the crystallinity and possibly the rearrangement of the atoms, and removal of defects becomes more accurate with increasing the solution volume [54]. As the spray

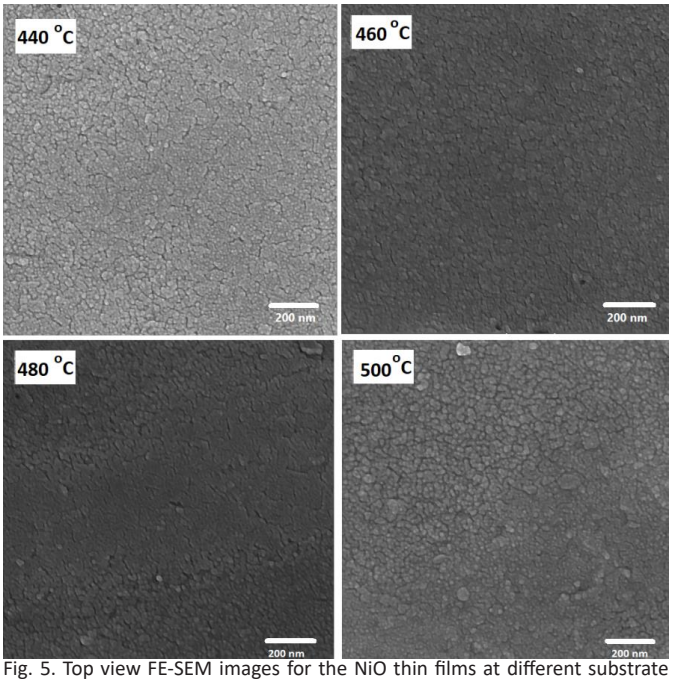

Fig. 5. Top view FE-SEM images for the NiO thin films at different substrate temperatures.

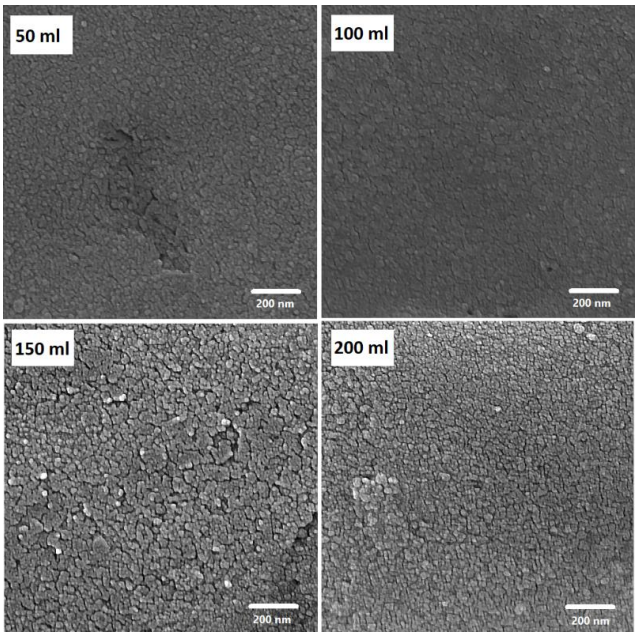

Fig. 6. Top view FE-SEM images for the NiO thin films with a different solution volume.

CC BY

rate increases, the values for average crystal grain size and dislocation density change, but these values are similar at spray rates of 1 ml/min and 7.5 ml/min.

FE-SEM is a suitable method to study the shape, size, and grain growth mechanism of particles. Figs. 5, 6, and 7 show the surface morphology of the NiO thin films prepared at different substrate temperatures, solution volumes, and spray rates, respectively. The FE-SEM morphologies of the NiO thin films are similar and exhibit spherical grains on their entire surface. The surface morphology of the deposited NiO film seems quasi-smooth, with excellent adhesion and uniform surface with densely packed spherical grains and utterly devoid of pinholes and major cracks on the film surface. A similar morphology is observed for NiO thin films reported in [56-59]. Moreover, the surface of the thin films is covered with inhomogeneous, randomly oriented, clustered particles. However, the morphology of the NiO thin films rests on the deposition parameters. Fig. 5 shows that the grains are condensed and large, and the surface uniformity improves when the substrate temperature increases from 440 to 500 °C[12, 13]. Fig. 6 shows the morphological inflections in thin films at a different solution volume. From the figure, it can be seen that the surface morphology of the thin films improves as the solution volume increases. Fig. 7 shows that the films are relatively porous, and no significant morphological change is observed as the spray rate increases. As shown in Figs. 5, 6, and 7, a smooth film with surface morphology is a basic requirement for applications in electronics, optoelectronics, and electrochromics [12, 57].

Figs. 8, 9, and 10 show two- and three-dimensional AFM microscopic images of thin films deposited at different substrate temperatures, solution volumes, and spray rates. The surface description results of the films are summarized in Table 2. The AFM images and the results of the average roughness values of the thin films facilitated our analysis of the physical properties of the thin films. These results show that the morphology of the thin films depends on the deposition conditions. Table 2 shows that an increase in substrate temperature leads to a decrease in the average roughness values of the thin films. On the other hand, increasing the solution volume leads to an increase in the average roughness values of the thin films. Increasing the spray rate from 1 ml/min to 7.5 ml/min leads first to a decrease and then to an increase in the

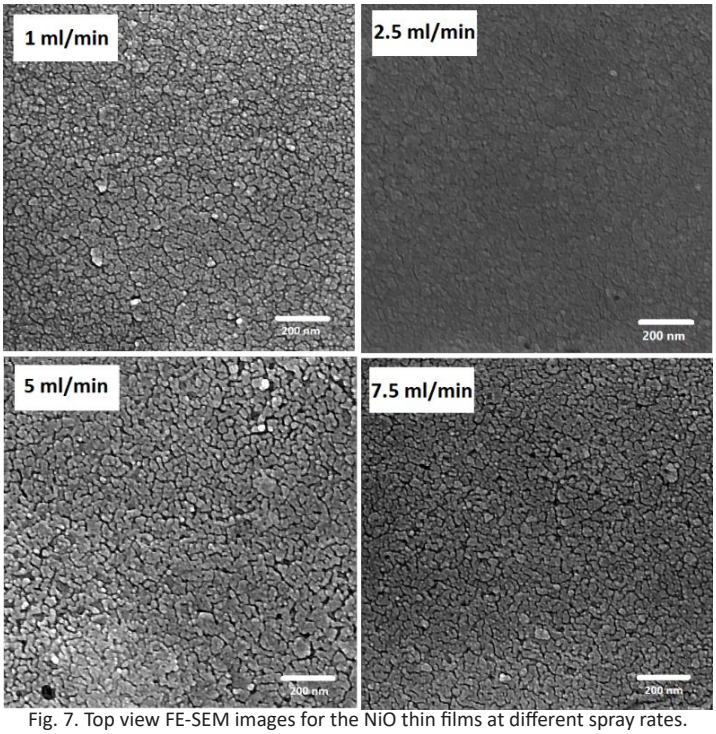

Fig. 7. Top view FE-SEM images for the NiO thin films at different spray rates.

CC BY

roughness values of the thin films.

Optical study

The exceptional optical properties of thin nickel oxide films make them suitable for a wide range of optoelectronic applications. Many of these applications require high transparency in the UV-vis region. This can be achieved by optimizing the parameters of the deposition layer, which play an important role in the optical properties of NiO thin films. These properties are related to the oxygen vacancy, surface roughness, structure, crystalline quality, grain size, and thickness of the deposited thin films [12, 18, 22, 43, 60-62]. Figs. 11, 12, and 13 show the optical transmission and absorption spectra of NiO thin films deposited at different substrate temperatures, solution volumes, and spray rates, respectively. All films were examined in the wavelength range of 300-1100 nm at room temperature. It can be seen that all films have an average transparency between 8% and 40% in the visible region. It was found that all the deposited samples have good transparency in the visible and near-infrared regions. In addition, the samples exhibit strong absorption in the UV range around 380 nm, which is consistent with previous studies [43]. At wavelengths below 380 nm, all samples show fundamental absorption related to the shift of electrons from the valence band to the conduction band [12, 27, 63-65].

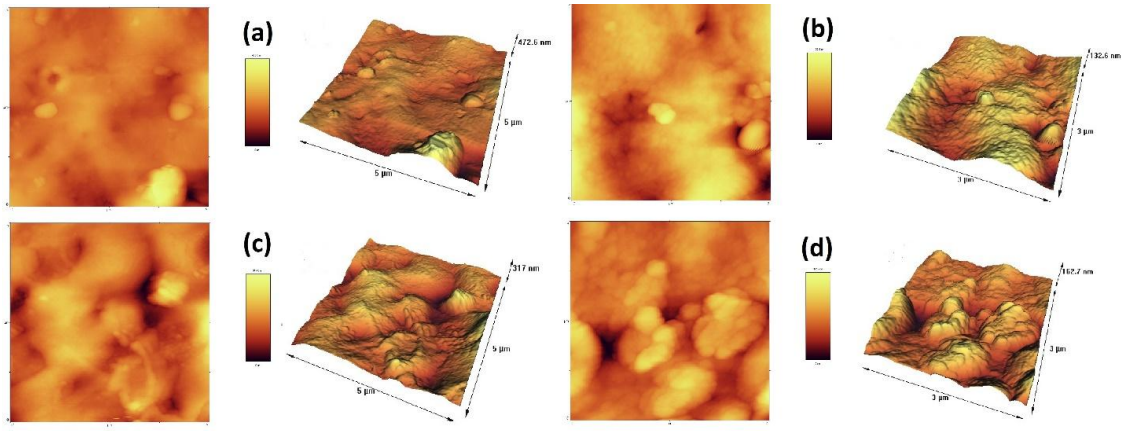

Fig. 8. AFM images for the NiO thin films at (a) 440, (b) 460, (c) 480, and (d) 500 oC substrate temperatures.

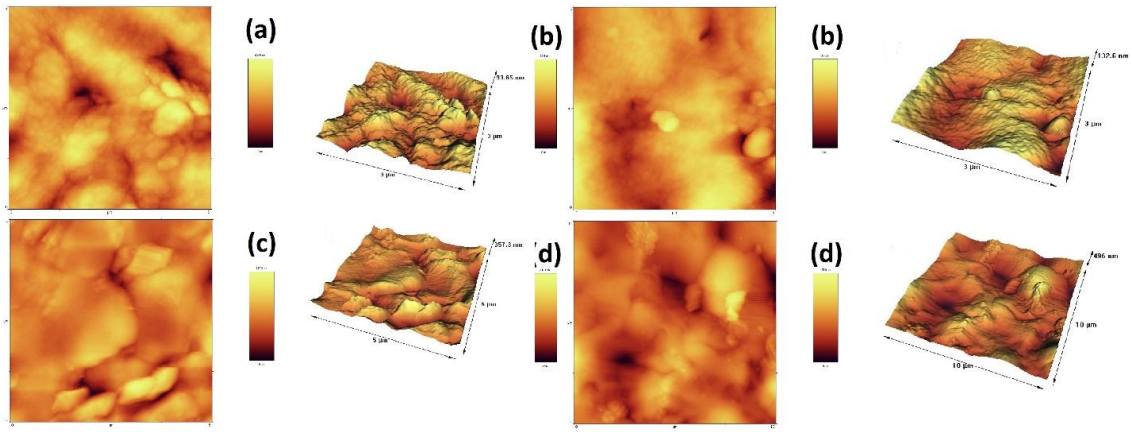

Fig. 9. AFM images for the NiO thin films at (a) 50, (b) 100, (c) 150, and (d) 200 ml solution volume.

CC BY

Fig. 11 shows that the optical transmittance of the thin films increases as the substrate temperature increases [47, 66]. This is because the thickness and surface roughness of the thin films decrease with an increase in the substrate temperature [22, 43]. Thus, the decreasing thickness and surface roughness of the films display less scattering of the incident light, followed with increased transmittance [11, 18, 42, 43, 67].

The absorption edge shifts slightly to the higher wavelength region as the solution volume

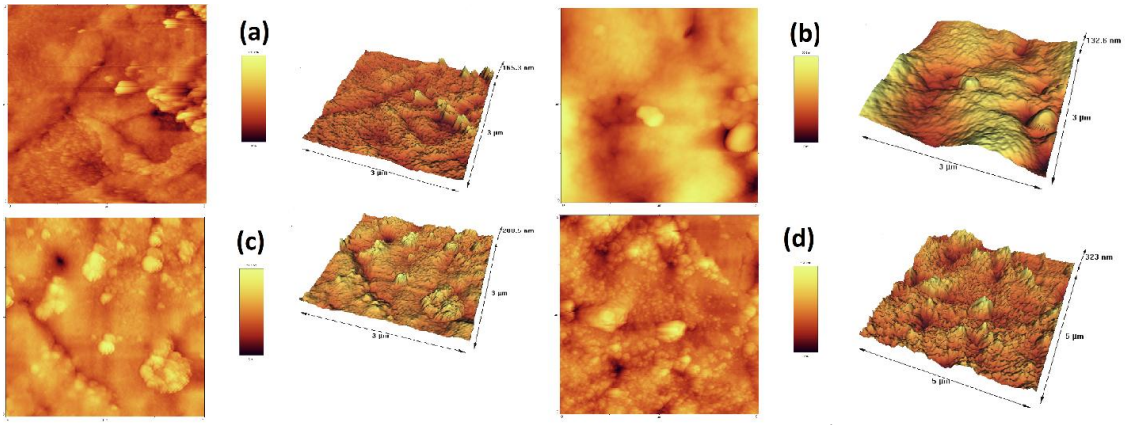

Fig. 10. AFM images for the NiO thin films at (a) 1, (b) 2.5, (c) 5, and (d) 7.5 ml/min spray rates.

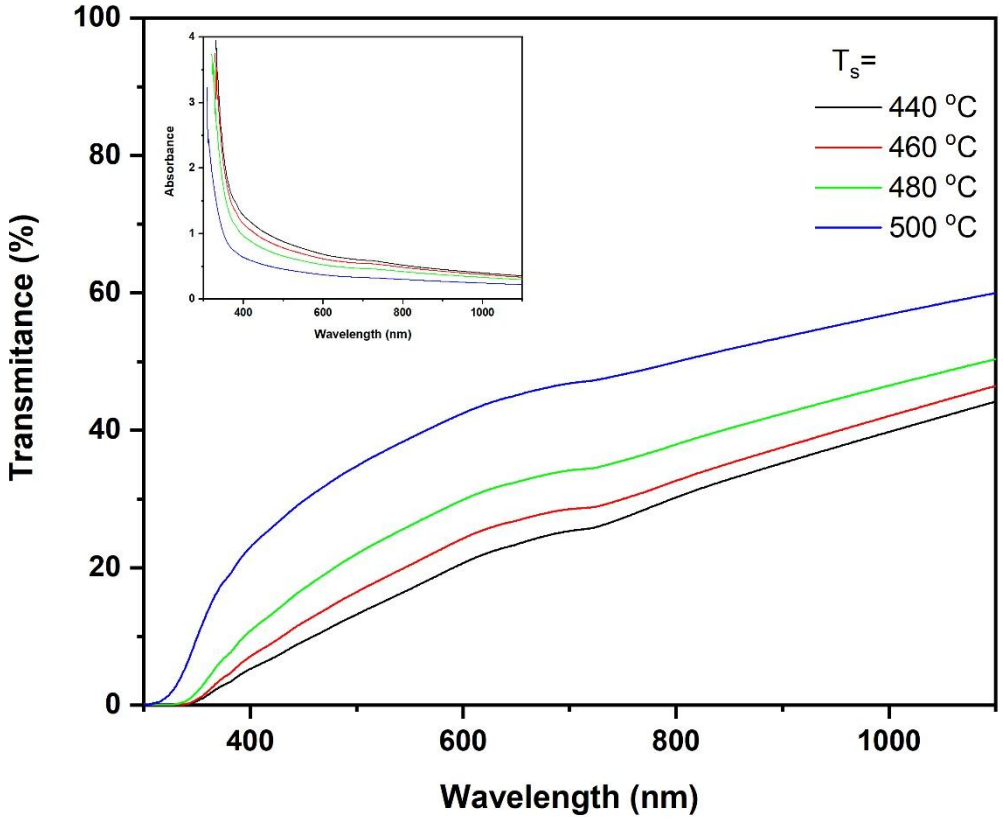

Fig. 11. The variation of transmittance and absorption as a function of wavelength for the NiO thin films at different substrate temperatures.

increases (see Fig. 12). This is attributed to the photoexcitation from the valence band to the conduction band. The film thickness increases as a function of the solution volume, leading to an increase in grain size and thus improved film coverage. Accordingly, the thicker films show

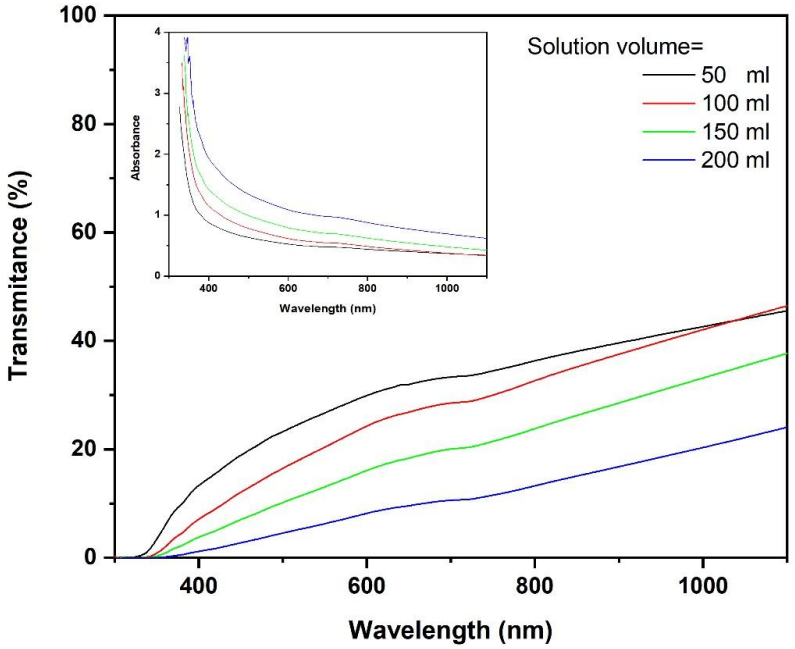

Fig. 12. The variation of transmittance and absorption as a function of wavelength for the NiO thin films at different solution volumes.

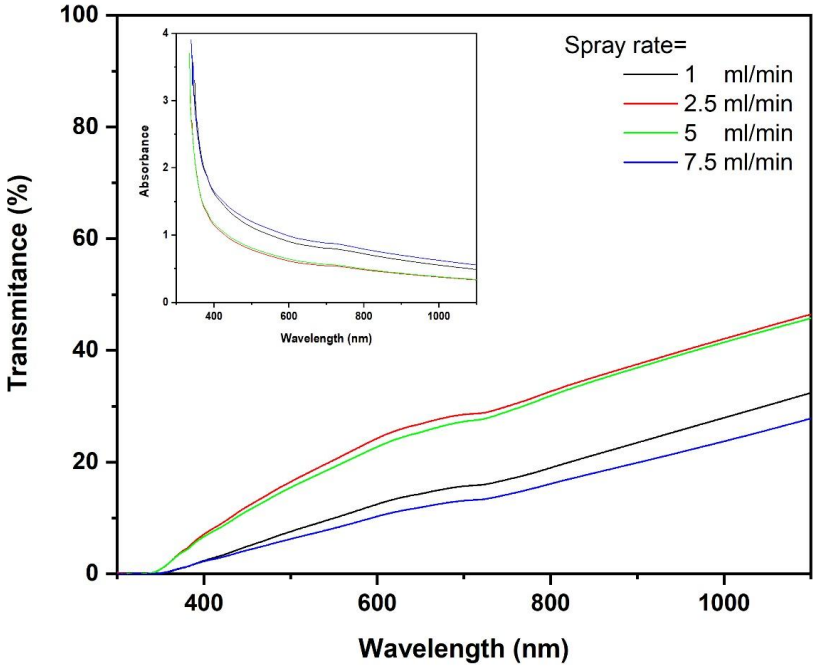

Fig. 13. The variation of transmittance and absorption as a function of wavelength for NiO thin films at different spray rates.

CC BY

more scattering of the incident light, resulting in lower transmittance [43]. Also, the increasing surface roughness with an increasing solution volume leads to decreasing transmittance. Thin film absorbance tends to decrease as wavelength gets higher. From the absorbance spectra, the absorption edge is found in the UV region at around 380 nm wavelength for all samples.

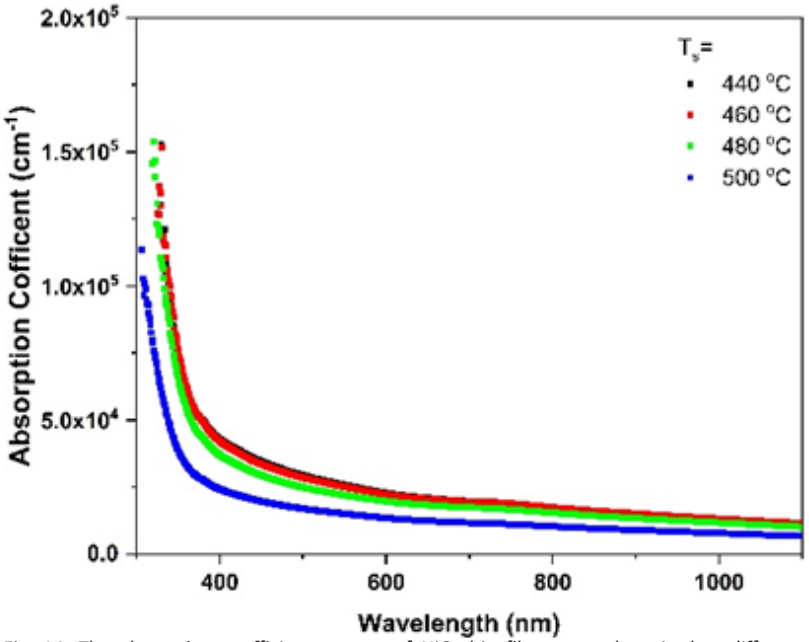

Fig. 14. The absorption coefficient spectra of NiO thin films were deposited at different substrate temperatures.

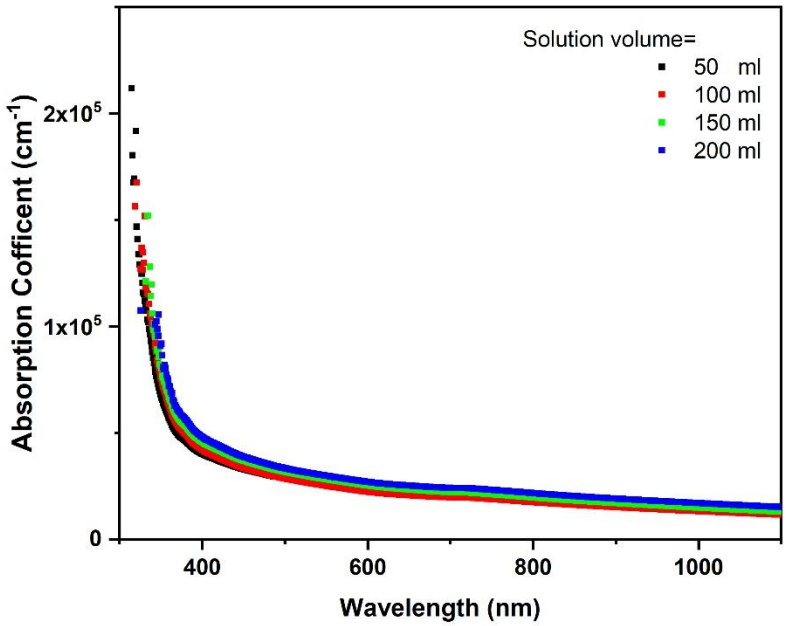

Fig. 15. The absorption coefficient spectra of NiO films deposited at different solution volumes.

CC BY

Optical absorption coefficients are calculated using the following formula [68]:

$$\alpha = \frac{1}{d}\ln\left(\frac{(1-R)^2}{T}\right) \quad (6)$$

where α, d, R, and T are the absorbance coefficient, thickness, reflectance, and transmittance of the thin films, respectively. Figs. 14, 15, and 16 show the absorbance coefficient spectra of the NiO thin films deposited at different substrate temperatures, solution volumes, and spray rates. Examination of these figures shows that the deposition parameters affect the absorbance coefficient. The thin films show a low absorbance coefficient in the visible region and

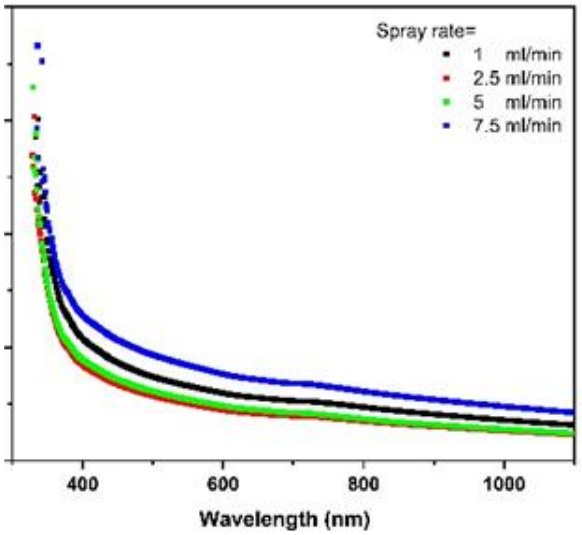

Fig. 16. The spectra of absorption coefficients of NiO films deposited at different spray rates.

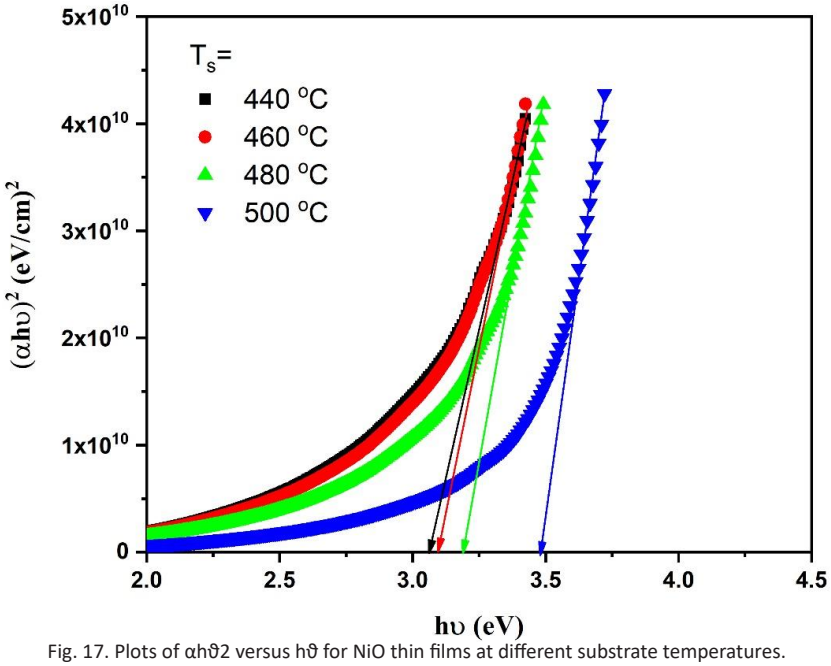

Fig. 17. Plots of αhϑ2 versus hϑ for NiO thin films at different substrate temperatures.

a strong absorbance coefficient in the regions of lower wavelength. Moreover, an absorption edge near (~380 nm) is observed in the thin films. The onset of remarkable absorption is in the wavelength region below 380 nm, which provides excellent transparency for thin films in the visible region. In general, the absorbance coefficient changes depending on the crystalline properties, band gap, surface roughness, and density of the defects [18, 23]. When the substrate temperature is lowered, or the the solution volume is increased, the absorption edges of thin films show a significant shift to longer wavelengths (red shift). This is due to the improved crystalline structure of the films that results from a decrease in the substrate temperature or an increase in the

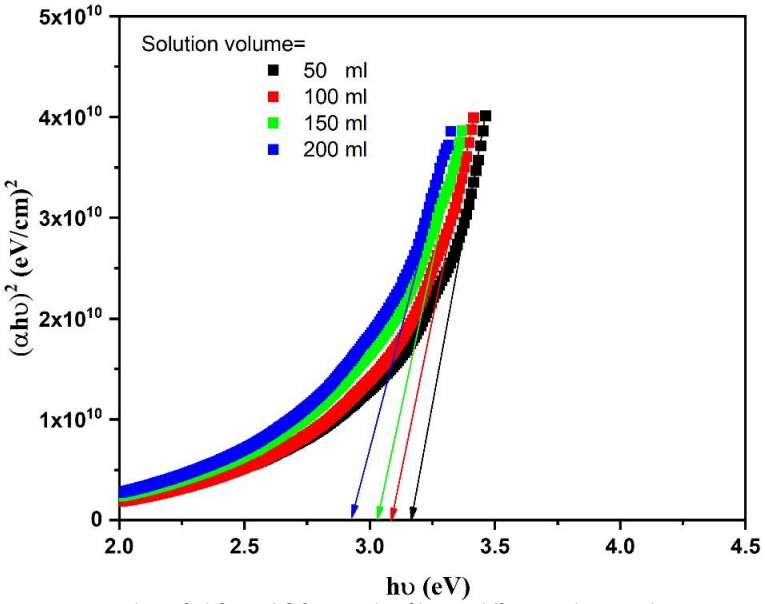

Fig. 18. Plots of αhϑ2 vs. hϑ for NiO thin films at different solution volumes.

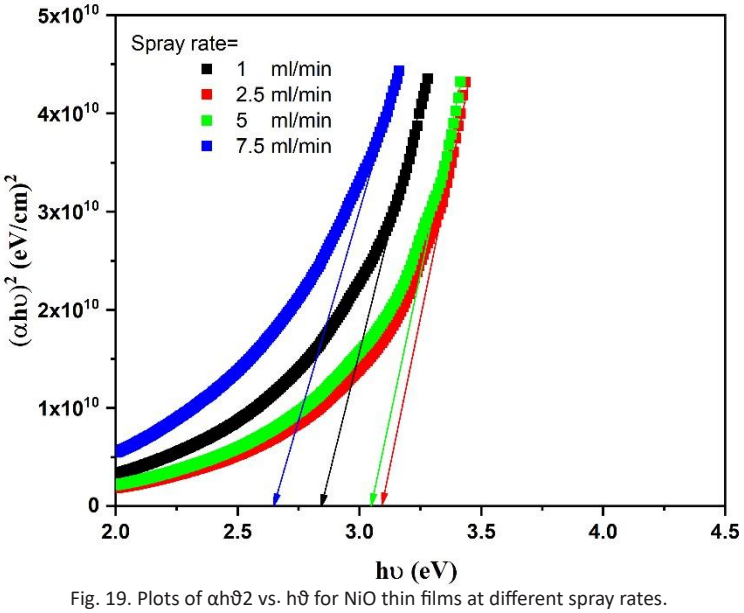

Fig. 19. Plots of αhϑ2 vs. hϑ for NiO thin films at different spray rates.

solution volume.

The direct optical band gap can be determined via optical absorption measurements by plotting $(\alpha h\upsilon)^2$ against the photon energy $h\vartheta$ and using the Tauc equation [69]:

$$(\alpha h\vartheta)^2 = \beta(h\vartheta - E_g) \quad (7)$$

where α, β, and E_g define the absorption coefficient, constant, and direct band gap, respectively, as shown in Figs. 17, 18, and 19 for the thin films prepared at different substrate temperatures, solution volumes, and spray rates, respectively. The band gap values are estimated to be in the range of 2.64 - 3.48 eV. The obtained band gap values agree well with previously reported data [12, 18, 21, 22, 43, 68, 70]. Increasing the thickness of the film causes a decrease in the band gap of the thin films as it makes the structure of the film better, as stated in the XRD analysis [24, 26, 39, 47]. Furthermore, an increase in the crystal grain size can decrease the band gap of the thin films because of the quantum size effect [26, 39, 63].

We can study the disorder of the thin films by the changes in absorption coefficients [68]. The

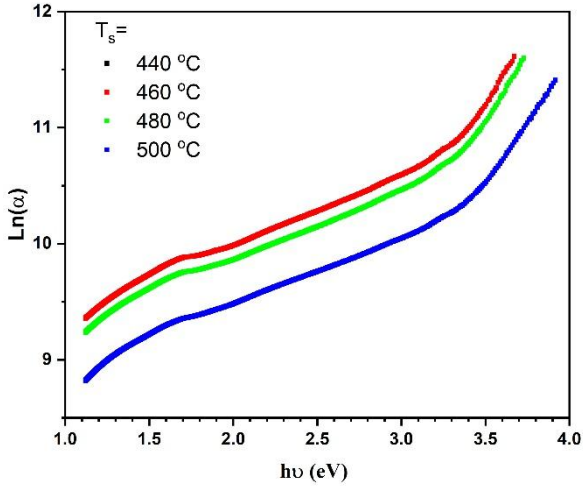

Fig. 20. Plots of ln(α) vs. hϑ for NiO thin films at different substrate temperatures.

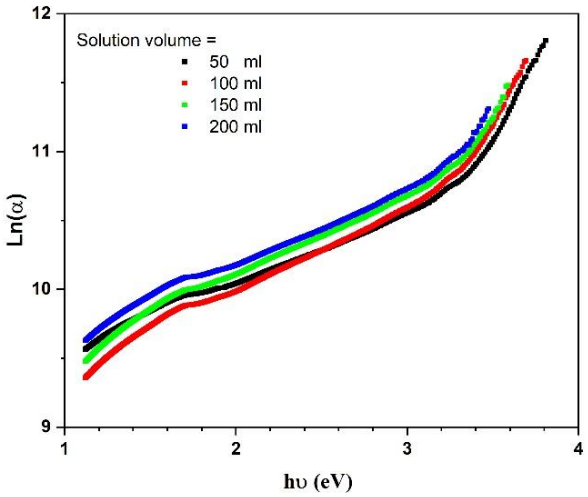

Fig. 21. Plots of ln(α) vs. hϑ for NiO thin films at different solution volumes.

CC BY

variation of the absorption coefficient with photon energy is given by the empirical Urbach low [71]:

$$\alpha = \alpha_o \exp\left(\frac{h\vartheta}{E_U}\right) \quad (8)$$

where α_o is a constant, $h\vartheta$ is the photon energy, and E_U is the Urbach energy. The Urbach energy is an important parameter characterizing the disorder and the width of the localized energy states in the material's band gap [25, 60, 65, 66]. The Urbach tail appears in poorly crystalline, disordered, and amorphous materials due to the localized states in these materials that widen or narrow the band gap [66]. Moreover, the interaction between charge carriers and phonons is responsible for the Urbach band tail in semiconductor materials [71]. The Urbach energy of the NiO thin films was estimated from the slopes of Ln(α) versus photon energy (hυ) plots. The inverted slope of Ln(α) versus photon energy (hυ) plots determine the values of the Urbach energy. Figs. 20, 21, and 22 show Ln(α) versus photon energy (hυ) plots of the thin films prepared at different substrate temperatures, solution volumes, and spray rates, respectively. We used these figures, determined the thin films' Urbach energy, and summarized them in Table 3. Furthermore, an increase in the crystal grain size can decrease the band gap of the thin films because of the quantum size effect [16, 60, 63].

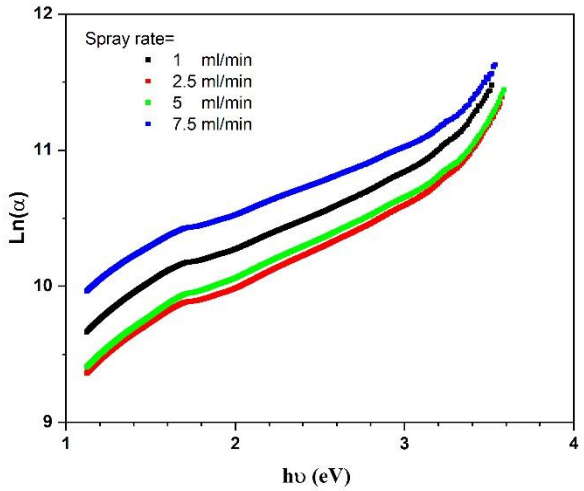

Fig. 22. Plots of ln(α) vs. hϑ for NiO thin films at different spray rates.

Table 3. The results of optical and electrical characterization of thin films.

Sample	t (nm)	Eg (eV)	Urbach energy (eV)	Sheet Resistance (×10^7 Ω/sq)	ρ (×10^3 Ω.cm)	n (×10^{14}cm^{-3})	μ (cm^2/v.s)
Substrate temperature (°)							
440	680	3.06	0.54	3.79	2.58	1.55	15.645
460	590	3.1	0.46	3.18	1.88	1.84	18.104
480	580	3.19	0.45	2.69	1.72	2.64	13.789
500	620	3.49	0.46	2.21	1.37	3.33	13.679
Solution volume (ml)							
50	490	3.16	0.41	4.82	2.36	2.81	9.417
100	590	3.1	0.46	3.18	1.88	1.84	18.104
150	620	3.03	0.47	2.21	1.37	3.33	13.697
200	820	2.92	0.45	1.63	1.34	3.64	12.84
Spray rate (ml/min)							
1	690	2.84	0.55	2.63	1.81	1.42	24.25
2.5	590	3.1	0.46	3.18	1.88	1.84	18.104
5	600	3.05	0.51	4.32	2.59	2.23	10.39
7.5	590	2.66	0.6	5.02	2.96	2.57	8.21

CC BY

The refractive index of the thin films is of great importance in designing optical components for spectral dispersion applications. The refractive index which is one of the most notable constants depends on the wavelength of the electromagnetic wave by dispersion. The refractive index delivers information about electronic polarization, local fields, and phase velocity of light propagating in the material [13]. It is a typical characteristic and fundamental property of any optical material. The optical characteristics such as the extinction coefficient (*k*) and refractive index (*n*) provide information about the polarization and structure of the thin films, which were papered at different parameter depositions. The extinction coefficient was calculated according to the relation [72]:

$$\alpha = \alpha_o \exp\left(\frac{h\vartheta}{E_U}\right) \quad (9)$$

The refractive index was calculated according to the relation [72]:

$$n = \left(\frac{1+R}{1-}\right) + \sqrt{\frac{4R}{(1-R)^2} - k^2} \quad (10)$$

From the equations, we can calculate the values of *n* and *k*. Figs. 23, 24, and 25 show the variations of the extinction coefficient and refractive index with the wavelength of the thin films deposited at different substrate temperatures, solution volumes, and spray rates. The extinction coefficient is a measurement of the portion of light loss as a result of scattering and absorption per unit distance of the medium penetration of the material [13]. The electronic polarization of ions and the local field within optical materials are closely connected to the refractive index [72]. Fig. 23 shows that the value of the extinction coefficient decreases with the substrate temperature as a result of the absorbance in NiO thin films decreases at higher temperatures [13]. The increase in (*n*) values may be because of the improvement in crystallinity and packing density of the NiO films as the substrate temperature or solution volume increases. The low values of *k* suggest that the prepared films have high optical transparency and improved surface homogeneity [62, 73, 74]. They lead to a decrease in the roughness of the film as the substrate temperature increases or the solution volume increases [62]. *K* and *n* values are expressed as significant constraints to study the electronic polarizability of the ions and the local field with respect to *λ* [75]. Such values of *k* for thin films make them favorites for optoelectronic devices. From the figure, it can be concluded that the value of the refractive index decreases as the solution volume increases in the low wavelength region [62]. Moreover, the extinction coefficient increases as the solution volume increases or the substrate temperature decreases, which agrees with the surface roughness measurement. This proposes that the surface roughness may take

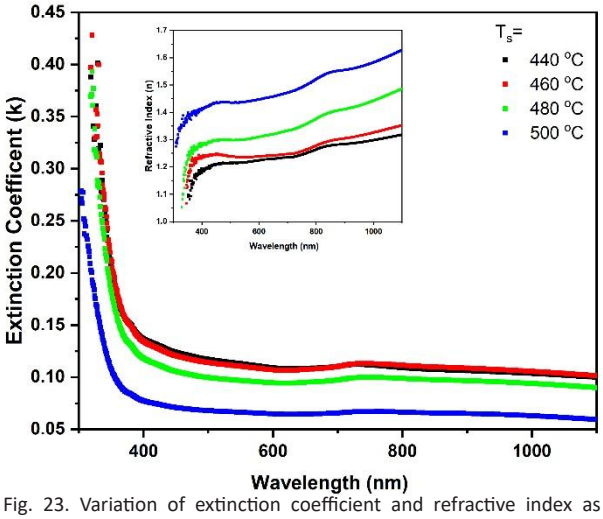

Fig. 23. Variation of extinction coefficient and refractive index as a function of wavelength of NiO thin films deposited at different substrate temperatures.

CC BY

part in the change in the extinction coefficient of the deposited films. Generally, the refractive index of a semiconductor is inversely proportional to the energy band gap [18]. This is also true in our case, where we observed lower values for the band gap and higher refractive indices as the solution volume increased [18]. The change in the refractive index with an increase in the substrate temperature may be the result of grain growth while the thin film deposits and a change in morphology, related to the change in extinction coefficient. The extinction coefficient measures the fraction of light loss caused by scattering and absorption per unit distance of the medium penetration of the material. The lowest value of (k) shows the lowest surface roughness, which results in decrease in scattering losses and increase in transmittance. Furthermore, a slight increase in the k value in the near-infrared region can be clarified by the metallic character of such thin oxide films [72].

The complex electronic dielectric constant describes the electron excitation spectrum of the thin films. It gives us information on the

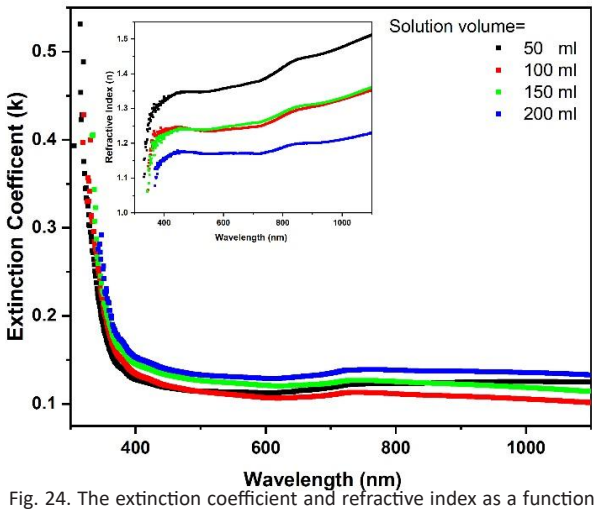

Fig. 24. The extinction coefficient and refractive index as a function of the wavelength of NiO thin film deposited at different solution volumes.

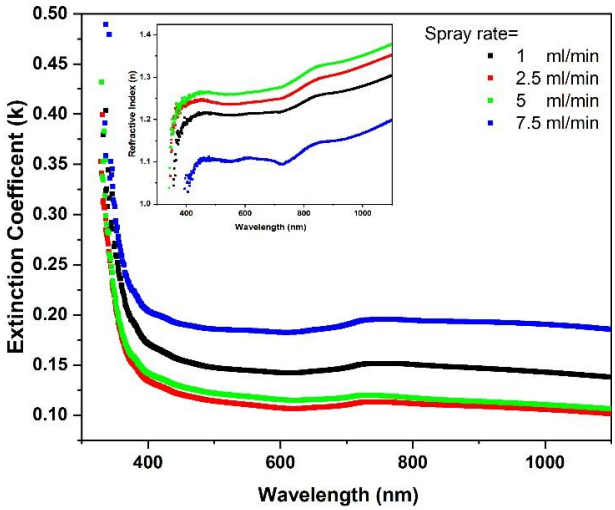

Fig. 25. The extinction coefficient and refractive index as a function of the wavelength of the NiO thin film deposited at different spray rates.

CC BY

permittivity of the material and the polarizability of a material which is related to the density of states in the forbidden gap. The imaginary part of the dielectric constant is necessary to understand the interaction of photons and electrons in thin films [70, 72]. The real and imaginary parts of the dielectric constant are defined as follows [1]:

$$\varepsilon_1 = n^2 - k^2 \quad (11)$$

$$\varepsilon_2 = 2nk \quad (12)$$

Where ε_1 and ε_2 are the real and imaginary

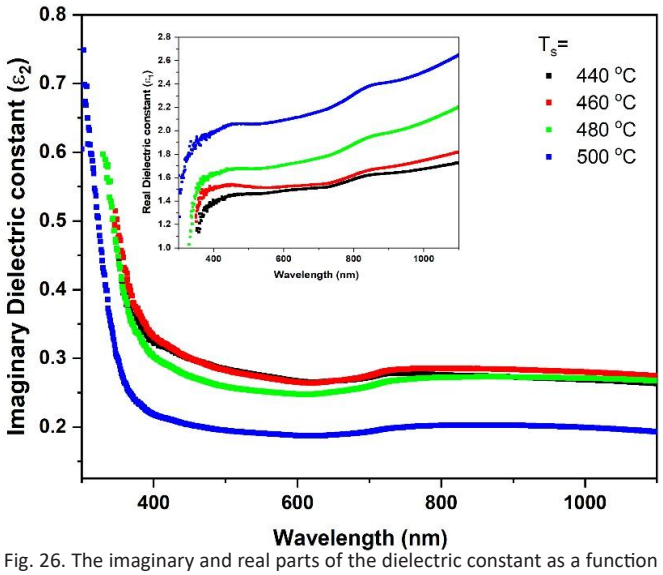

Fig. 26. The imaginary and real parts of the dielectric constant as a function of the wavelength of the NiO thin film deposited at different substrate temperatures.

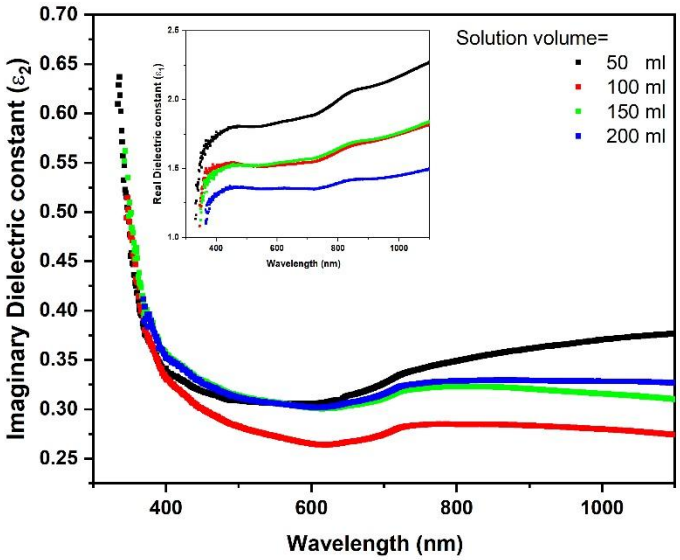

Fig. 27. The imaginary and real parts of the change in dielectric constant as a function of the wavelength of the NiO thin film deposited at different solution volumes.

CC BY

parts of the dielectric constant, *n* is the refractive index, and *k* is the extinction coefficient.

The variation of the real and imaginary dielectric constants with wavelength is shown in Figs. 26, 27, and 28 for the thin films deposited at various substrate temperatures, solution volumes, and spray rates, respectively. Inspection of these figures shows that the variation of the dielectric constants with the incident photon energy proves an exchange between the incident photons and the free electrons in the studied wavelength range [13]. Moreover, these constants show similar behavior to *k* and *n*. The figures also show that the values of the real part are higher than those of the imaginary part $\varepsilon_1 > \varepsilon_2$ [13, 68, 70, 72, 74]. The real part of the dielectric constant increased as the substrate temperature increased, while the imaginary part of the dielectric constant decreased as the substrate temperature increased. This behavior is reversed for thin films with an increased solution volume.

The calculation of optical conductivity can help us study the optical resonance of the material and identify the allowed interband optical transitions in it [13, 16]. This is useful since it makes the electronic density of states available in the materials, the conductivity of a material in the presence of incident photons, and the optical response of the material [13, 62, 68]. By using the following formula the optical conductivity of the thin films is calculated [68]:

$$\sigma_p = \frac{\alpha n c}{4\pi} \tag{13}$$

where, α, n and c are the absorption coefficient, refractive index, and velocity of light, respectively. The behavior of the optical conductivities as a function of the photon energy of the thin films deposited at different substrate temperatures, solution volumes, and spray rates, respectively, is shown in Figs. 29, 30, and 31. By looking at the figures, it can be understood that the optical conductivity of all samples increases as a function of photon energy [68].

The excitation of electrons could explain this by photon energy [68]. The thin films have a very high and stable value of σ_p in the order of 10^{14} s^{-1} in the energy range of 2.6 - 3.8 eV. The high and stable value of σ_p in the mentioned energy range confirms that the prepared films have good photoreaction [16, 62]. It was discovered that the optical conductivity increases with the substrate temperature, which is the result of the electrons movement from the valence band to the conduction band that occurs when photons of certain wavelengths strike the NiO thin films [13].

Electrical properties

The electrical properties at room temperature were measured and are summarized in Table 3. The

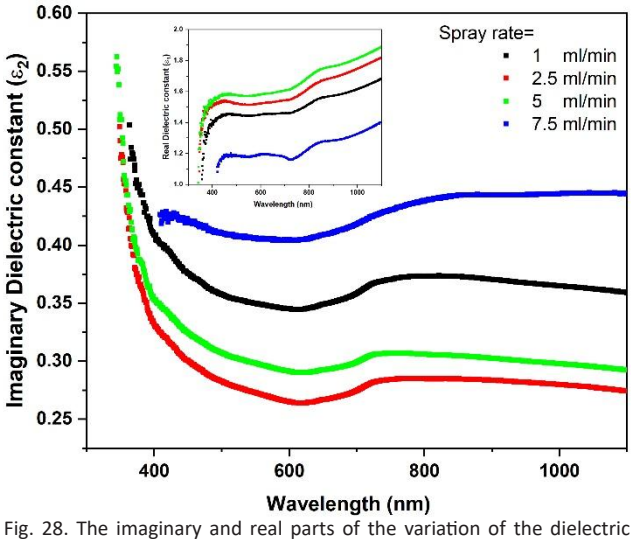

Fig. 28. The imaginary and real parts of the variation of the dielectric constant as a function of the wavelength of the NiO thin film deposited at different spray rates.

compositional change, particularly the formation of Ni^{+2} vacancies, leads to a p-type conductivity of the thin films [5, 76, 77]. This is due to two Ni^{2+} ions must be converted to Ni^{3+} to sustain the crystal's overall electrical neutrality. Thus, Ni^{2+} vacancies are at the origin of the hole conductivity of NiO since each Ni^{2+} vacancy is replaced by two Ni^{3+} ions [5, 24].

The electrical resistivity of the thin films is in the range of 1.33×10^{3} to 2.96×10^{3} Ω cm, as reported by many researchers [50]. The resistivity of the NiO films decreases as the substrate temperature increases and the solution volume increases. In contrast, it decreases when the rate increases.

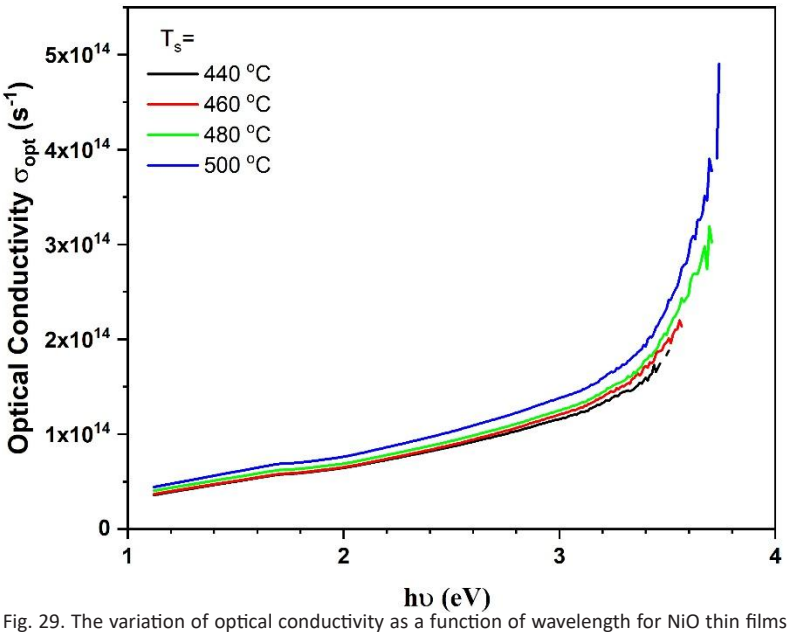

Fig. 29. The variation of optical conductivity as a function of wavelength for NiO thin films deposited at different substrate temperatures.

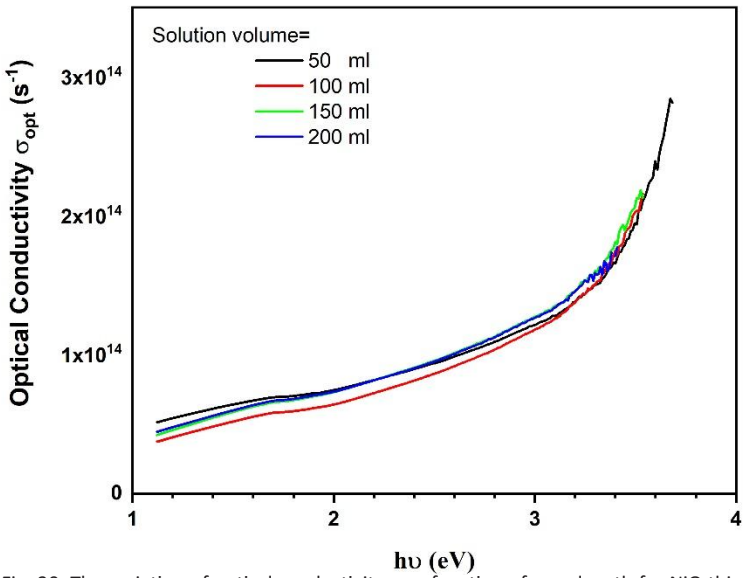

Fig. 30. The variation of optical conductivity as a function of wavelength for NiO thin films deposited with different solution volumes.

CC BY

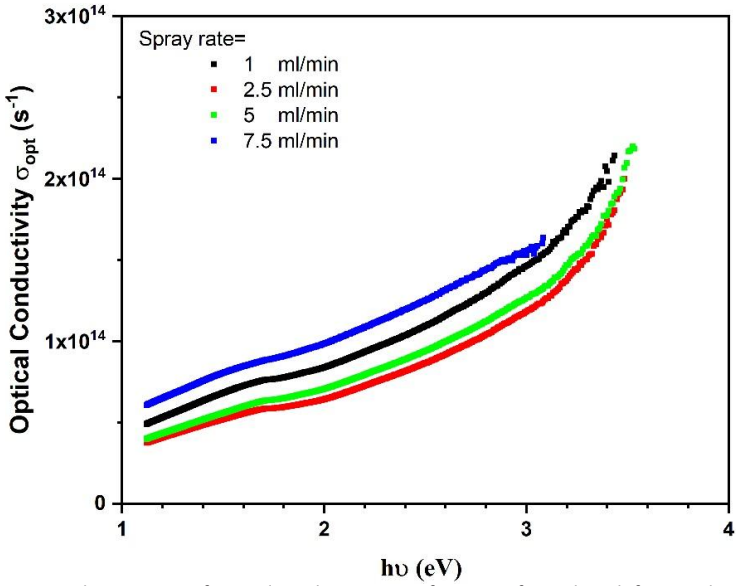

Fig. 31. The variation of optical conductivity as a function of wavelength for NiO thin films deposited at different spray rates.

This is probably because of the formation of a nonstoichiometric film with excess or less oxygen [50]. The mechanism of electrical conductivity of NiO can be related to the existence of localized Ni^{3+} in the NiO lattice. So, the increase in the resistivity of the thin films can be the result of an increase in ions due to the added oxygen, which might lead to the formation of nickel vacancies or interstitial oxygen in NiO crystallites [24].

Therefore, microstructural defects such as Ni vacancies and interstitial O affect resistivity by acting as scattering centers in the NiO lattice Moreover, an increase in the grain size causes an improved crystalline structure and consequently a decrease in the resistivity of the NiO thin films [50, 65]. The carrier concentration is generally increased by increasing the substrate temperature, solution volume, and spray rate. These improvements lead to a decrease in ionized impurities, which in turn leads to an increase in hole carrier concentration [24]. The values of carrier mobility are presented in Table 3. The carrier mobility (μ) was affected by the grain boundary scattering (μ_{GB}) and the scattering of ionized impurities (μ_{GB}). This was derived using the equation $1/\mu=1/\mu_{GB}+1/\mu_{IS}$. This indicates that the carrier mobility decreases due to an increase in the grain boundary and impurities (Ni vacancies and relatively larger interstitial O) [77]. In addition, carrier mobility increases due to a decrease in the scattering centers of the impurities [24].

CONCLUSION

We prepared NiO thin films by spray pyrolysis on glass substrates with different deposition conditions in the present work. The effect of the substrate temperature, solution volume, and spray rate on the structural, optical, and electrical properties of the films was investigated using XRD, FE-SEM, AFM, UV-vis spectroscopy and Hall effect analysis. The structural analysis showed that the films have a cubic structure. The refractive index, extinction coefficient, and dielectric constants were calculated, and the values agreed well with the literature. Increasing the substrate temperature decreased the average roughness, Urbach energy, electrical resistivity, and carrier mobility on the one hand, and increased the optical cap and carrier concentration on the other. In general, increasing the solution volume increased the average roughness, Urbach energy, carrier concentration, and carrier mobility on the one hand, and decreased the optical cap and electrical resistivity on the other. In general, increasing the spray rate decreased the average roughness, optical gap, and carrier mobility and increased Urbach energy, electrical resistivity, and carrier concentration. The thin films exhibited p-type conduction, making them suitable for solar

CC BY

cells. The thin films exhibited p-type conduction, making them suitable for solar cells. We have shown that the physical properties of NiO thin films can be developed for use in optoelectronic devices.

CONFLICT OF INTEREST

The authors declare that there is no conflict of interests regarding the publication of this manuscript.

REFERENCES

1. Ganesh V. Effect of Bi doping on the structural and optical properties of NiO thin films. Optics and Laser Technology. 2022;146:107579.
2. Terlemezoglu M, Surucu O, Isik M, Gasanly NM, Parlak M. Temperature-dependent optical characteristics of sputtered NiO thin films. Appl Phys A. 2021;128(1).
3. Yousefi M, Noori E, Ghanbari D, Salavati-Niasari M, Gholami T. A Facile Room Temperature Synthesis of Zinc Oxide Nanostructure and Its Influence on the Flame Retardancy of Poly Vinyl Alcohol. J Cluster Sci. 2013;25(2):397-408.
4. Parkhomenko HP, Solovan MN, Mostovoi AI, Orletskii IG, Parfenyuk OA, Maryanchuk PD. Optical and electrical properties of thin NiO films deposited by reactive magnetron sputtering and spray pyrolysis. Opt Spectrosc. 2017;122(6):944-948.
5. Cheemadan S, Santhosh Kumar MC. Effect of substrate temperature and oxygen partial pressure on RF sputtered NiO thin films. Materials Research Express. 2018;5(4):046401.
6. Usha KS, Sivakumar R, Sanjeeviraja C, Ichimura M. Physical properties of rf magnetron sputter deposited NiO:WO_3 thin films. Materials Research Express. 2014;2(1):016401.
7. Ksapabutr B, Nimnuan P, Panapoy M. Dense and uniform NiO thin films fabricated by one-step electrostatic spray deposition. Mater Lett. 2015;153:24-28.
8. Gomaa MM, Yazdi GR, Schmidt S, Boshta M, Khranovskyy V, Eriksson F, et al. Effect of precursor solutions on the structural and optical properties of sprayed NiO thin films. Mater Sci Semicond Process. 2017;64:32-38.
9. Kaya S. Nanostructure, optical and electrical properties of p-NiO/n-Si heterojunction diodes. Appl Phys A. 2020;126(8).
10. Lin Y-J, Su T-H, Kuo P-C, Chang H-C. A source of free holes in NiO thin films with different nickel content that are prepared using the sol-gel method. Materials Chemistry and Physics. 2022;276:125345.
11. Ganesh V, Kumar BR, Bitla Y, Yahia IS, AlFaify S. Structural, Optical and Dielectric Properties of Nd Doped NiO Thin Films Deposited with a Spray Pyrolysis Method. Journal of Inorganic and Organometallic Polymers and Materials. 2021;31(6):2691-2699.
12. Visweswaran S, Venkatachalapathy R, Haris M, Murugesan R. Structural, morphological, optical and magnetic properties of sprayed NiO thin films by perfume atomizer. Appl Phys A. 2020;126(7).
13. Kate RS, Bulakhe SC, Deokate RJ. Effect of Substrate Temperature on Properties of Nickel Oxide (NiO) Thin Films by Spray Pyrolysis. J Electron Mater. 2019;48(5):3220-3228.
14. Kumar M. Effect of substrate temperature on surface morphology and optical properties of sputter deposited nanocrystalline nickel oxide films. Materials Research Express. 2019;6(9):096404.
15. Ashok Kumar Reddy Y, Sivasankar Reddy A, Sreedhara Reddy P. Influence of oxygen partial pressure on the structural, optical and electrical properties of Cu-doped NiO thin films. Phys Scr. 2012;87(1):015801.
16. Aftab M, Butt MZ, Ali D, Bashir F, Khan TM. Optical and electrical properties of NiO and Cu-doped NiO thin films synthesized by spray pyrolysis. Opt Mater. 2021;119:111369.
17. Hotovy I, Rehacek V, Kemeny M, Ondrejka P, Kostic I, Mikolasek M, et al. Preparation and gas-sensing properties of very thin sputtered NiO films. Journal of Electrical Engineering. 2021;72(1):61-65.
18. Sharma R, Acharya AD, Shrivastava SB, Patidar MM, Gangrade M, Shripathi T, et al. Studies on the structure optical and electrical properties of Zn-doped NiO thin films grown by spray pyrolysis. Optik. 2016;127(11):4661-4668.
19. Akl AA, Mahmoud SA. Effect of growth temperatures on the surface morphology, optical analysis, dielectric constants, electric susceptibility, Urbach and bandgap energy of sprayed NiO thin films. Optik. 2018;172:783-793.
20. Ahmed AA, Afzal N, Devarajan M, Subramani S. Structural, morphological, optical and electrical properties of NiO films prepared on Si (100) and glass substrates at different thicknesses. Materials Research Express. 2016;3(11):116405.
21. Shajudheen VPM, Kumar VS, Maheswari AU, Sivakumar M, Kumar SS, Rani KA. Characterization and anticorrosion studies of spray coated nickel oxide (NiO) thin films. Materials Today: Proceedings. 2018;5(2):8577-8586.
22. Sharma R, Acharya AD, Shrivastava SB, Shripathi T, Ganesan V. Preparation and characterization of transparent NiO thin films deposited by spray pyrolysis technique. Optik. 2014;125(22):6751-6756.
23. Mrabet C, Ben Amor M, Boukhachem A, Amlouk M, Manoubi T. Physical properties of La-doped NiO sprayed thin films for optoelectronic and sensor applications. Ceram Int. 2016;42(5):5963-5978.
24. Menaka SM, Umadevi G. Concentration Dependent Structural, Morphological, Spectral, Optical and Electrical Properties of Spray Pyrolyzed NiO thin films. Silicon. 2018;10(5):2023-2029.
25. Loukil A, Boukhachem A, Ben Amor M, Ghamnia M, Raouadi K. Effects of potassium incorporation on the structural, optical, vibrational and electrical properties of NiO sprayed thin films for p-type optical windows. Ceram Int. 2016;42(7):8274-8289.
26. Balakarthikeyan R, Santhanam A, Anandhi R, Vinoth S, Al-Baradi AM, Alrowaili ZA, et al. Fabrication of nanostructured NiO and NiO:Cu thin films for high-performance ultraviolet photodetector. Opt Mater. 2021;120:111387.
27. Aoun Y, Marrakchi M, Benramache S, Benhaoua B, Lakel S, Cheraf A. Preparation and Characterizations of Monocrystalline Na Doped NiO Thin Films. Materials Research. 2018;21(2).
28. Kaya D, Aydınoğlu HS, Şenadım Tüzemen E, Ekicibil A. Investigation of optical, electronic, and magnetic properties of p-type NiO thin film on different substrates. Thin Solid Films. 2021;732:138800.
29. Nongjai R, Asokan K. Structural and optical properties of Ni implanted NiO thin films. AIP Conference Proceedings: AIP Publishing; 2020. p. 030321.
30. Lin C-W, Chung W-C, Zhang Z-D, Hsu M-C. P-channel transparent thin-film transistor using physical-vapor-deposited NiO layer. Jpn J Appl Phys. 2017;57(1S):01AE01.

CC BY

31. Fasaki I, Kandyla M, Kompitsas M. Properties of pulsed laser deposited nanocomposite NiO:Au thin films for gas sensing applications. Appl Phys A. 2012;107(4):899-904.
32. Şenaslan F, Taşdemir M, Çelik A. Effect of working pressure and post-annealing on structural, optical and electrical properties of p-type NiO thin films produced by RF magnetron sputtering technique. Appl Phys A. 2021;127(10).
33. Matienzo DJD, Settipani D, Instuli E, Kallio T. Active IrO2 and NiO Thin Films Prepared by Atomic Layer Deposition for Oxygen Evolution Reaction. Catalysts. 2020;10(1):92.
34. Perumal R, Thanikaikarasan S. Thickness, structural and optical properties of electrodeposited NiO thin films. Materials Today: Proceedings. 2020;33:3989-3992.
35. J A, Sahoo T. Effect of Li doping on conductivity and band gap of nickel oxide thin film deposited by spin coating technique. Materials Research Express. 2019;7(1):016405.
36. Li Y, Zhao GY, Kou ZB, Liu JC, Zhu R. Study on Resistive Switching Property of Ti Doped Novel NiO Thin Films. IOP Conference Series: Materials Science and Engineering. 2018;303:012007.
37. Gund GS, Lokhande CD, Park HS. Controlled synthesis of hierarchical nanoflake structure of NiO thin film for supercapacitor application. J Alloys Compd. 2018;741:549-556.
38. Roffi TM, Nozaki S, Uchida K. Growth mechanism of single-crystalline NiO thin films grown by metal organic chemical vapor deposition. J Cryst Growth. 2016;451:57-64.
39. Das MR, Mukherjee A, Mitra P. Structural, optical and ac electrical characterization of CBD synthesized NiO thin films: Influence of thickness. Physica E: Low-dimensional Systems and Nanostructures. 2017;93:243-251.
40. Martinez-Luevanos A, Oliva J, Garcia CR, Avalos-Belmontes F, Garcia-Lobato MA. Effect of cobalt on the electrochromic properties of NiO films deposited by spray pyrolysis. Appl Phys A. 2017;123(5).
41. Qin Y, Song J, Qiu Q, Liu Y, Zhao Y, Zhu L, et al. High-quality NiO thin film by low-temperature spray combustion method for perovskite solar cells. J Alloys Compd. 2019;810:151970.
42. Hakkoum H, Tibermacine T, Sengouga N, Belahssen O, Ghougali M, Benhaya A, et al. Effect of the source solution quantity on optical characteristics of ZnO and NiO thin films grown by spray pyrolysis for the design NiO/ZnO photodetectors. Opt Mater. 2020;108:110434.
43. Gomaa MM, Sayed MH, Patil VL, Boshta M, Patil PS. Gas sensing performance of sprayed NiO thin films toward NO2 gas. J Alloys Compd. 2021;885:160908.
44. Fadavieslam MR. A study of the structural, optical, and electrical properties of SnS_2:Cu optical semiconductor thin films deposited by the spray pyrolysis technique. Journal of Materials Science: Materials in Electronics. 2016;28(3):2392-2400.
45. Ukoba KO, Eloka-Eboka AC, Inambao FL. Review of nanostructured NiO thin film deposition using the spray pyrolysis technique. Renewable and Sustainable Energy Reviews. 2018;82:2900-2915.
46. Kate RS, Khalate SA, Deokate RJ. Electrochemical properties of spray deposited nickel oxide (NiO) thin films for energy storage systems. J Anal Appl Pyrolysis. 2017;125:289-295.
47. Boukhachem A, Boughalmi R, Karyaoui M, Mhamdi A, Chtourou R, Boubaker K, et al. Study of substrate temperature effects on structural, optical, mechanical and opto-thermal properties of NiO sprayed semiconductor thin films. Materials Science and Engineering: B. 2014;188:72-77.
48. Kate RS, Khalate SA, Deokate RJ. Synthesis and characterization of nickel oxide (NiO) thin films. AIP Conference Proceedings: Author(s); 2017. p. 080048.
49. Salunkhe P, A.V MA, Kekuda D. Structural, spectroscopic and electrical properties of dc magnetron sputtered NiO thin films and an insight into different defect states. Appl Phys A. 2021;127(5).
50. Patil PS, Kadam LD. Preparation and characterization of spray pyrolyzed nickel oxide (NiO) thin films. Appl Surf Sci. 2002;199(1-4):211-221.
51. Deepa P, Philominathan P. Influence of substrate temperature on certain physical properties and antibacterial activity of nanocrystalline Ag-doped In_2O_3 thin films. Pramana. 2016;87(6).
52. Anbarasi M, Nagarethinam V, Balu A. Investigations on the structural, morphological, optical and electrical properties of undoped and nanosized Zn-doped CdS thin films prepared by a simplified spray technique. Materials Science-Poland. 2014;32(4):652-660.
53. Sajilal K, Moses Ezhil Raj A. Effect of thickness on physico-chemical properties of p-NiO (bunsenite) thin films prepared by the chemical spray pyrolysis (CSP) technique. Optik. 2016;127(3):1442-1449.
54. Sajilal K, Ezhil Raj AM. Effect of thickness on structural and magnetic properties of NiO thin films prepared by chemical spray pyrolysis (CSP) technique. Mater Lett. 2016;164:547-550.
55. Abbasi L, Hedayati K, Ghanbari D. Magnetic properties and kinetic roughening study of prepared polyaniline: lead ferrite, cobalt ferrite and nickel ferrite nanocomposites electrodeposited thin films. Journal of Materials Science: Materials in Electronics. 2021;32(11):14477-14493.
56. Mani Menaka S, Umadevi G, Manickam M. Effect of copper concentration on the physical properties of copper doped NiO thin films deposited by spray pyrolysis. Materials Chemistry and Physics. 2017;191:181-187.
57. Özütok F, Demiri S, Özbek E. Electrochromic NiO thin films prepared by spin coating. AIP Conference Proceedings: Author(s); 2017. p. 050011.
58. Dong D, Djaoued H, Vienneau G, Robichaud J, Brown D, Brüning R, et al. Electrochromic and colorimetric properties of anodic NiO thin films: Uncovering electrochromic mechanism of NiO. Electrochimica Acta. 2020;335:135648.
59. Manouchehri I, AlShiaa SAO, Mehrparparvar D, Hamil MI, Moradian R. Optical properties of zinc doped NiO thin films deposited by RF magnetron sputtering. Optik. 2016;127(20):9400-9406.
60. Diha A, Benramache S, Benhaoua B. Transparent nanostructured Co doped NiO thin films deposited by sol–gel technique. Optik. 2018;172:832-839.
61. Atak G, Coşkun ÖD. Annealing effects of NiO thin films for all-solid-state electrochromic devices. Solid State Ionics. 2017;305:43-51.
62. Shkir M, Ganesh V, AlFaify S, Yahia IS, Zahran HY. Tailoring the linear and nonlinear optical properties of NiO thin films through Cr^{3+} doping. Journal of Materials Science: Materials in Electronics. 2018;29(8):6446-6457.
63. Kumar A, Sahay PP. Lithium doping in spray-pyrolyzed NiO thin films: results on their microstructural, optical and electrochromic properties. Appl Phys A. 2021;127(4).
64. Barir R, Benhaoua B, Benhamida S, Rahal A, Sahraoui T, Gheriani R. Effect of Precursor Concentration on Structural Optical and Electrical Properties of NiO Thin Films Prepared

CC BY

by Spray Pyrolysis. Journal of Nanomaterials. 2017;2017:1-10.
65. Maaoui B, Aoun Y, Benramache S, Nid A, Far R, Touati A. Synthesis and Characterization of Physical Properties of the NiO Thin Films by Various Concentrations. Advances in Materials Science. 2020;20(3):79-87.
66. Jamal MS, Shahahmadi SA, Chelvanathan P, Alharbi HF, Karim MR, Ahmad Dar M, et al. Effects of growth temperature on the photovoltaic properties of RF sputtered undoped NiO thin films. Results in Physics. 2019;14:102360.
67. Paul Joseph D, Saravanan M, Muthuraaman B, Renugambal P, Sambasivam S, Philip Raja S, et al. Spray deposition and characterization of nanostructured Li doped NiO thin films for application in dye-sensitized solar cells. Nanotechnology. 2008;19(48):485707.
68. Khalidi ZE, Fadili S, Hartiti B, Lfakir A, Thevenin P, Siadat M. Behavior of NiO thin films sprayed at different annealing time. Optical and Quantum Electronics. 2016;48(9).
69. Raj ILP, Valanarasu S, Abdeltawab AA, Mohammady SZ, Ubaidullah M, Shaikh SF, et al. Improved UV photosensing properties of high crystalline nickel oxide thin films: Role of yttrium doping. Optik. 2021;248:168105.
70. Alshahrie A, Yahia IS, Alghamdi A, Al Hassan PZ. Morphological, structural and optical dispersion parameters of Cd-doped NiO nanostructure thin film. Optik. 2016;127(12):5105-5109.
71. Chandoul F, Moussa H, Jouini K, Boukhachem A, Hosni F, Fayache MS, et al. Investigation of the properties of nanostructured nickel oxide NiO thin films irradiated at different γ-doses. Journal of Materials Science: Materials in Electronics. 2018;30(1):348-358.
72. Kate RS, Bulakhe SC, Deokate RJ. Co doping effect on structural and optical properties of nickel oxide (NiO) thin films via spray pyrolysis. Optical and Quantum Electronics. 2019;51(10).
73. Benhamida S, Gouamid M, Tlili S, Khenblouche A, Charradi K. Structural, optical and dielectric properties of Zn-doped NiO thin films synthesized via sol-gel route. Digest Journal of Nanomaterials and Biostructures. 2021;16(2):433-442.
74. Ganesh V, Haritha L, Anis M, Shkir M, Yahia IS, Singh A, et al. Structural, morphological, optical and third order nonlinear optical response of spin-coated NiO thin films: An effect of N doping. Solid State Sciences. 2018;86:98-106.
75. Shkir M, Arif M, Ganesh V, Singh A, Algarni H, Yahia IS, et al. An effect of Fe on physical properties of nanostructured NiO thin films for nonlinear optoelectronic applications. Appl Phys A. 2020;126(2).
76. Guillén C, Herrero J. Influence of Acceptor Defects on the Structural, Optical and Electrical Properties of Sputtered NiO Thin Films. physica status solidi (a). 2021;218(16).
77. Oh S, Park YS, Ko PJ, Kim N-H. Effects of Rapid Thermal Treatment on Characteristics of Magnetron-Sputtered NiO Thin Films for Supercapacitor Applications. Journal of Nanoscience and Nanotechnology. 2018;18(9):6213-6219.

CC BY